Eur. Phys. J. D **38**, 353–365 (2006)
DOI: 10.1140/epjd/e2006-00015-5

THE EUROPEAN PHYSICAL JOURNAL D

Atom interferometry measurement of the electric polarizability of lithium

A. Miffre, M. Jacquey, M. Büchner, G. Trénec, and J. Vigué[a]

Laboratoire Collisions Agrégats Réactivité, IRSAMC, Université Paul Sabatier and CNRS UMR 5589, 118 route de Narbonne, 31062 Toulouse Cedex, France

Received 29 July 2005 / Received in final form 2nd December 2005
Published online 17 January 2006 –

Abstract. Using an atom interferometer, we have measured the static electric polarizability of ^{7}Li $\alpha = (24.33 \pm 0.16) \times 10^{-30}$ m^3 $= 164.2 \pm 1.1$ atomic units with a 0.66% uncertainty. Our experiment, which is similar to an experiment done on sodium in 1995 by Pritchard and co-workers, consists in applying an electric field on one of the two interfering beams and measuring the resulting phase-shift. With respect to Pritchard's experiment, we have made several improvements which are described in detail in this paper: the capacitor design is such that the electric field can be calculated analytically; the phase sensitivity of our interferometer is substantially better, near 16 mrad/$\sqrt{\text{Hz}}$; finally our interferometer is species selective so that impurities present in our atomic beam (other alkali atoms or lithium dimers) do not perturb our measurement. The extreme sensitivity of atom interferometry is well illustrated by our experiment: our measurement amounts to measuring a slight increase Δv of the atom velocity v when it enters the electric field region and our present sensitivity is sufficient to detect a variation $\Delta v/v \approx 6 \times 10^{-13}$.

PACS. 32.10.Dk Electric and magnetic moments, polarizability – 03.75.Dg Atom and neutron interferometry – 32.60.+i Zeeman and Stark effects – 39.20.+q Atom interferometry techniques

1 Introduction

The measurement of the electric polarizability α of an atom is a difficult experiment: this quantity cannot be measured by spectroscopy, which can access only to polarizability differences, and one should rely either on macroscopic quantity measurements such as the electric permittivity (or the index of refraction) or on electric deflection of an atomic beam. For a review on polarizability measurements, we refer the reader to the book by Kresin and Bonin [1]. For alkali atoms, all the accurate experiments were based on the deflection of an atomic beam by an inhomogeneous electric field and, in the case of lithium, the most accurate previous measurement was done in 1974 by Bederson and co-workers [2], with the following result $\alpha = (24.3 \pm 0.5) \times 10^{-30}$ m^3. However, in 2003, Amini and Gould, using an atomic fountain [3], have measured the polarizability of cesium atom with a 0.14% relative uncertainty, which is presently the smallest uncertainty on the electric polarizability of an alkali atom.

Atom interferometry, which can measure any weak modification of the atom propagation, is perfectly adapted to measure the electric polarizability of an atom: this was demonstrated in 1995 by Pritchard and co-workers [4] with an experiment on sodium atom and they obtained a very high accuracy, with a statistical and systematic uncertainties both equal to 0.25%. This experiment was and remains difficult because an electric field must be applied on only one of the two interfering beams: one must use a capacitor with a thin electrode, a septum, which can be inserted between the two atomic beams.

Using our lithium atom interferometer [5,6], we have made an experiment very similar to the one of Pritchard [4] and we have measured the electric polarizability of lithium with a 0.66% uncertainty, limited by the uncertainty on the mean atom velocity and not by the atom interferometric measurement itself [8]. In the present paper, we are going to describe in detail our experiment with emphasis on the improvements with respect to the experiments of Pritchard's group [4,9]: we have designed a capacitor with an analytically calculable electric field; we have obtained a considerably larger phase sensitivity, thanks to a large atomic flux and an excellent fringe visibility; finally our interferometer, which uses laser diffraction, is species selective: the contribution of any impurity (heavier alkali atoms, lithium dimers) to the signal can be neglected.

We may recall that several experiments using atom interferometers have exhibited a sensitivity to an applied electric field [10–12] but these experiments were not aimed at an accurate measurement of the electric polarizability. Two other atom interferometry experiments [13,14] using

[a] e-mail: jacques.vigue@irsamc.ups-tlse.fr

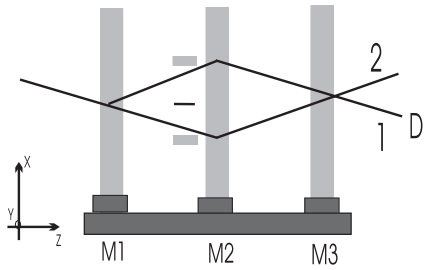

Fig. 1. Schematic drawing of our experiment based on a Mach-Zehnder atom interferometer: a collimated atomic beam, coming from the left, is diffracted by three laser standing waves made by reflecting three laser beams on the mirrors M_1, M_2 and M_3. The output beam labeled 1 is selected by a slit and detected by a hot-wire detector D. The capacitor with a septum between the two interfering beams is placed just before the second laser standing wave. The x, y and z-axis are defined.

an inelastic diffraction process, so that the two interfering beams are not in the same internal state, have measured the difference of polarizability between these two internal states. Finally, two experiments [15–17] have measured the Aharonov-Casher phase [18]: this phase, which results from the application of an electric field on an atom with an oriented magnetic moment, is proportional to the electric field.

This paper is organized as follows. We briefly recall the principle of the experiment in Section 2. We then describe our electric capacitor in Section 3 and the experiment in Section 4. The analysis of the experimental data is done in Section 5 and we discuss the polarizability result in Section 6. A conclusion and two appendices complete the paper.

2 Principle of the measurement

If we apply an electric field E on an atom, the energy of its ground state decreases by the polarizability term:

$$U = -2\pi\epsilon_0\alpha E^2. \tag{1}$$

When an atom enters a region with a non vanishing electric field, its kinetic energy increases by $-U$ and its wave vector k becomes $k + \Delta k$, with Δk given by $\Delta k = 2\pi\epsilon_0\alpha E^2 m/(\hbar k)$. The resulting phase shift ϕ of the atomic wave is given by:

$$\phi = \frac{2\pi\epsilon_0\alpha}{\hbar v}\int E^2(z)dz \tag{2}$$

where we have introduced the atom velocity $v = \hbar k/m$ and taken into account the spatial dependence of the electric field along the atomic path following the z-axis. This phase shift is inversely proportional to the atom velocity and this dependence will be included in our analysis of the results.

The principle of the experiment, illustrated in Figure 1, is to measure this phase shift by applying an electric field on one of the two interfering beams in an atom interferometer [4]. This is possible only if the two beams are spatially separated so that a septum can be inserted between the two beams. This requirement could be suppressed by using an electric field with a gradient as in reference [9] but it seems difficult to use this arrangement for a high accuracy measurement, because an accurate knowledge of the values of the field and of its gradient at the location of the atomic beams would be needed.

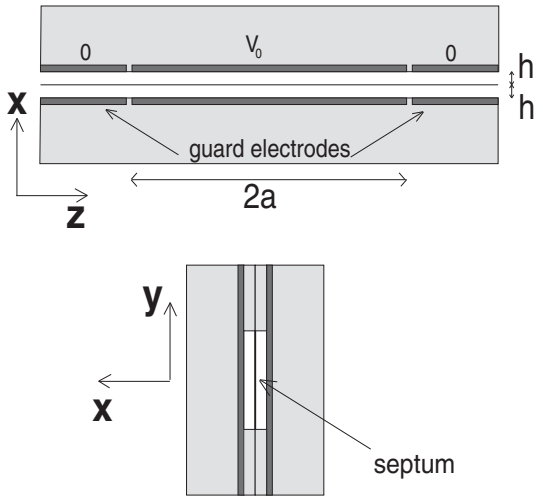

Fig. 2. Two schematic drawings of the capacitor: top view of the capacitor cut in the atomic beam plane (upper panel) and end view as seen by an observer located on the atomic beam (lower panel). The axis being the same as in Figure 1, the septum and the electrodes are parallel to the y, z plane, with the septum at $x = 0$ and the electrodes at $x = \pm h$. The high voltage electrodes at the $V = V_0$ potential extends from $z = -a$ to $z = +a$, while the guard electrodes extend outside with $|z| > a$. The septum and the guard electrodes are at the $V = 0$ potential.

3 The electric capacitor

3.1 Capacitor design

To make an accurate measurement, we must know precisely the electric field along the atomic path and guard electrodes are needed so that the length of the capacitor is well defined, as discussed by Pritchard and co-workers [4]. It would probably be better to have guard electrodes on both electrodes, but it seems very difficult to draw guard electrodes on the septum and to put them in place very accurately. Therefore, as in reference [4], we have guard electrodes only on the massive electrodes. However, we have chosen to put our guard electrodes in the plane of the high voltage electrode. With this choice, the calculation of the electric field can be done analytically. Figure 2 presents two schematic drawings of the capacitor and defines our notations, while an artist's view is presented in Figure 3. Like in reference [4], our capacitor is as symmetric as possible with respect to the septum plane, but, for a given experiment, only one half of the capacitor is used, the other part creating no electric field with $V = 0$ everywhere.

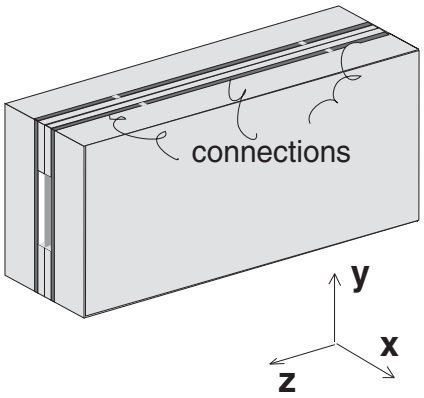

Fig. 3. Artist's view of the capacitor: we have also shown schematically some wires connecting the electrodes, the important point being that these wires are not close to the atomic beams.

3.2 Calculation of the capacitor electric field

3.2.1 From three dimensions to two dimensions

If a dielectric slab with a permittivity $\epsilon_r > 1$ is introduced in a plane capacitor, the field lines are distorted and concentrated towards the slab. Because our capacitor contains dielectric spacers, one could fear a similar effect but this effect does not exist when the dielectric slab fills completely the gap between the electrodes. Following Figure 2, the spacers, with a dielectric constant ε_r, completely fill the space $|y| > y_0$, with vacuum in the rest of capacitor, $|y| < y_0$. Let V (respectively V_1) be the potential with $|y| < y_0$ ($|y| > y_0$). In the $|y| = y_0$ planes, the continuity equations give:

$$V = V_1 \quad \text{and} \quad \frac{\partial V}{\partial y} = \frac{\partial V_1}{\partial y} \tag{3}$$

As shown below, a 2D solution of the Laplace equation of the form $V(x, z)$ exists for the capacitor. Then clearly, if we take $V_1 = V$, this solution fulfills both continuity equations on the dielectric borders in the $|y| = y_0$ planes and we know that the solution is unique.

3.2.2 Calculation of the potential and of the electric field

We consider only one half (with $x \geq 0$) of the capacitor represented in Figure 2. We know the potential on the borders of the capacitor, with $V(x = 0, z) = 0$ and $V(x = h, z) = V_0$ if $|z| < a$ and $V(x = h, z) = 0$ if $|z| > a$. To get the potential everywhere, we start by calculating the Fourier transform $\tilde{V}(k)$ of $V(x = h, z)$:

$$\tilde{V}(k) = \frac{1}{\sqrt{2\pi}} \int_{-\infty}^{+\infty} V(x = h, z) \exp(-ikz)\, dz. \tag{4}$$

Then, for a separable harmonic function of x and z, with a z-dependence of the $\exp(ikz)$ form, its x-dependence is necessarily given by a linear combination of the two functions $\exp(\pm kx)$. Using this result and the conditions on the borders at $x = 0$ and at $x = h$, we get the value of $V(x, z)$ everywhere:

$$V(x, z) = \frac{1}{\sqrt{2\pi}} \int_{-\infty}^{+\infty} \tilde{V}(k) \frac{\sinh(kx)}{\sinh(kh)} \exp(ikz)\, dk \tag{5}$$

from which we can deduce the electric field everywhere. On the septum surface $x = 0$, the electric field is parallel to the x-axis and we can calculate exactly the integral of E^2 on this surface (see Appendix A). We need the capacitor effective length L_{eff} which is defined by:

$$L_{eff} = \frac{1}{E_0^2} \int_{-\infty}^{+\infty} E^2 dz \tag{6}$$

where $E_0 = V_0/h$ is the electric field of an infinite plane capacitor with the same electrode spacing h. Using equation (28), we get the exact value of L_{eff}:

$$L_{eff} = 2a \left[\coth\left(\frac{\pi a}{h}\right) - \frac{h}{\pi a} \right] \approx 2a - \frac{2h}{\pi} \tag{7}$$

where exponentially small corrections of the order of $\exp[-2\pi a/h]$ have been neglected in the approximate result.

However, the atoms do not sample the electric field on the septum surface but at a small distance, of the order of 50 μm in our experiment, and what we need is the integral of E^2 along their mean trajectory. This mean trajectory is not exactly parallel to the septum, but it is easier to calculate the integral along a constant x line. We may use either the potential given by equation (5) or Maxwell's equations to relate the field components near the septum surface to its value on the surface. The calculation, given in Appendix A, proves that the first correction to the effective length is proportional to x^2:

$$L_{eff} \approx 2a - \frac{2h}{\pi} + \frac{2\pi x^2}{3h}. \tag{8}$$

The x^2 correction is a fraction of the main term $2a$ equal to $\pi x^2/(3ah)$ and with our dimensions ($x \approx 50$ μm, $h \approx 2$ mm and $a \approx 25$ mm), this correction is close to $5 \times 10^{-5} L_{eff}$. This correction is negligible at the present level of accuracy and we will use the value of L_{eff} given by the approximate form of equation (7). More precisely, we will write:

$$\int_{-\infty}^{+\infty} E^2 dz = V_0^2 \left[\frac{2a}{h^2} - \frac{2}{\pi h} \right]. \tag{9}$$

3.3 Construction of the capacitor

Let us describe how we build this capacitor. The external electrodes are made of glass plates (80 mm long in the z-direction, 35 mm high in the y-direction, 10 mm thick in the x-direction) covered by an evaporated aluminium layer. To separate the guard electrodes from the high voltage electrode, a gap is made in the aluminium layer by

laser evaporation [19]. We found that 100 μm wide gaps give a sufficient insulation under vacuum to operate the capacitor up to $V_0 = 500$ V. These gaps are separated by a distance $2a = 50$ mm, so that the two guard electrodes are 15 mm long. The glass spacers are $\sim$2 mm thick plates of float glass (10 mm $\times$ 80 mm) used without further polishing. The distance y_0 from the spacer inner edge to the atomic beam axis is equal to $\sim$7 mm.

We have found that a float glass plate is flat within ± 2 μm over the needed surface. This accuracy appeared to be sufficient for a first construction, as the main geometrical defects are due to the way we assemble the various parts by gluing them together and by an imperfect stretching of the septum. We use a double-faced tape ARCLAD 7418 (from Adhesive Research) to assemble the spacers on the external electrodes.

The septum is made of 6 μm thick mylar from Goodfellow covered with aluminium on both faces. In a first step, the mylar sheet is glued on a circular metal support. It is then covered by a thin layer of dish soap diluted in water and the mylar is heated near 80 °C with a hot air gun. Then, we clean the mylar surface with water and let it dry. After this operation, the mylar is well stretched and its surface is very flat. We have measured the resonance frequencies of the drum thus formed, from which we deduced a surface tension of the order of 50 N/m (this value is only indicative as this experiment was made with another mylar film which was 20 μm thick). Once stretched, the mylar film is glued on one electrode-spacer assembly with an epoxy glue EPOTEK 301 (from Epoxy Technology), chosen for its very low viscosity, and then it is cut with a scalpel. In a final step, a second electrode-spacer assembly is glued on the other face of the mylar. Finally, as shown in Figure 3, wires are connected to the various electrodes using an electrically conductive adhesive EPOTEK EE129-4 (also from Epoxy Technology).

3.4 Residual defects of the capacitor

We are going to discuss the various points by which the real capacitor differs from our model.

3.4.1 2D character of the potential

We have shown that the potential V is reduced to a 2D function when an homogeneous dielectric slab fills completely the gap between the electrodes, with the border between the vacuum and the slab being a plane perpendicular to the electrodes. The real dielectric slab is the superposition of a tape, a glass spacer and a glue film, each material having a different permittivity ϵ_r. The differences in permittivity perturb the potential which should take a 3D character extending on a distance comparable to the tape or glue film thicknesses. This perturbation seems negligible, because the tape and the glue films are very thin and also because these three dielectric materials have not very large ϵ_r values.

3.4.2 Do we know the potential everywhere on the border?

Our calculation assumes that the potential is known everywhere on the border. But, on the high-voltage electrode, we may fear that the potential is not well defined in the 100 μm wide dielectric gaps separating the high voltage and guard electrodes as these gaps might get charged in an uncontrolled way. This is not likely if the volume resistivity ρ of the Pyrex glass used is not too large: more precisely, the time constant for the charge equilibration on the gap surface is given by $\epsilon_0 \rho$ (within numerical factors of the order of one) and this time constant remains below 1 second if $\rho \leq 10^{11}$ Ω m. We have found several values of the resistivity of Pyrex glass at ordinary temperature, in the range $(4\text{–}8) \times 10^8$ Ω m and with such a conductivity, this time constant is below 10^{-2} s. Our calculation neglects the surface conductivity, due to the adsorbed impurities, which should further reduce this time constant.

Therefore, we think that it is an excellent approximation to assume that the potential V makes a smooth transition from $V = 0$ to $V = V_0$ in the gaps. Then, using equation (26), it is clear that the detailed shape of the transition has no consequence as these details are smoothed out by the convolution of $V(z)$ by the function $g(z)$ which has a full width at half maximum equal to $1.12h$. We can use equation (7) to calculate the effective length, provided that we add to the length of the high voltage electrode the mean width of the two gaps. In the present work, we have taken one gap width, 100 μm, as a conservative error bar on the effective length. A superiority of our capacitor design is that these gaps are very narrow, thus minimizing the corresponding uncertainty on the capacitor effective length and we hope to be able to further reduce this uncertainty.

3.4.3 Parallelism of the electrodes

The thickness h of the capacitor, which is the sum of the thickness of the spacers, the tape and the glue film, is not perfectly constant. Using a Mitutoyo Litematic machine, we have measured, with a ± 1 μm uncertainty, the capacitor thickness as a function of z, in the center line of the two spacers, at $y = \pm 12$ mm. The average of these two measurements gives the thickness $h(z)$ in the $y = 0$ plane around which the atom sample the electric field. The thickness h is not perfectly constant but it is well represented by a linear function of z, given by $h(z) = h_0 + h_1(z/a)$, the maximum deviation h_1 being considerably smaller than the mean h value noted h_0. As these deviations are very small (see below), it seems reasonable to use equation (9) provided that terms involving powers of h are replaced by their correct averages. The first term in h^{-2} corresponds to the integral of E^2 over the capacitor length, from $z = -a$ to $z = a$ and we must take the average value of h^{-2} over this region. Neglecting higher order terms, this average is given by:

$$\left\langle \frac{1}{h^2} \right\rangle = \frac{1}{h_0^2} \left[1 + \frac{h_1^2}{h_0^2} \right]. \tag{10}$$

In equation (9), the second term in h^{-1}, corresponds to end effects and this quantity must be replaced by the following two-point average:

$$\left\langle \frac{1}{h} \right\rangle = \frac{1}{2}\left(\frac{1}{h(z=-a)} + \frac{1}{h(z=a)} \right) = \frac{1}{h_0}\left[1 + \frac{h_1^2}{h_0^2} \right]. \tag{11}$$

Both corrections involve the same factor $[1 + (h_1^2/h_0^2)]$.

3.4.4 Summary of the capacitor dimensions

Although the capacitor is as symmetric as possible, this symmetry is only approximate and we give the parameters for the half we have used for the set of measurements described below. The length of the high voltage electrode, including one gap width is $2a = 50.00 \pm 0.10$ mm, the error bar being taken equal to one gap width, as discussed above. The distance h between the electrodes gap width is described by $h_0 = 2.056 \pm 0.003$ mm and $h_1 = 3.2 \times 10^{-3}$ mm. The correction term $h_1^2/h_0^2 = 2.4 \times 10^{-6}$ is completely negligible.

4 The experiment

In this part, we are going to recall the main features of our lithium atom interferometer, to give the values of various parameters used for the present study, to present the data acquisition procedure and the way we extract the phases from the data.

4.1 Our interferometer

Our atom interferometer is a Mach-Zehnder interferometer using Bragg diffraction on laser standing waves. Its design is inspired by the sodium interferometer of Pritchard and co-workers [20,21] and by the metastable neon interferometer of Siu Au Lee and co-workers [22]. A complete description has been published [5,6].

The lithium atomic beam is a supersonic beam seeded in argon and, for the present experiment, we have worked with a low argon pressure in the oven $p_0 = 167$ mbar, because the detected lithium signal increases when the argon pressure decreases. The oven body temperature is equal to 973 K, fixing the vapor pressure of lithium at $p_{\mathrm{Li}} = 0.8$ mbar and the nozzle temperature is equal to $T_0 = 1073$ K. With these source conditions, following our detailed analysis [7], the argon and lithium velocity distributions are described by a parallel speed ratio for argon equal to $S_{\parallel,\mathrm{Ar}} = 8.3$ and a parallel speed ratio for lithium equal to $S_{\parallel,\mathrm{Li}} = 6.2$ (the parallel speed ratio is defined by equation (15) below).

We use Bragg diffraction on laser standing waves at $\lambda = 671$ nm: the laser is detuned by about 3 GHz on the blue side of the $^2\mathrm{S}_{1/2} - {}^2\mathrm{P}_{3/2}$ transition of the ^{7}Li isotope, the signal is almost purely due to this isotope, which has a natural abundance equal to 92.41%, and not to the other isotope ^{6}Li. Moreover, any other species present in the beam, for instance heavier alkali atoms or lithium dimers, is not diffracted and does not contribute to the signal.

The case of lithium dimers deserves a special discussion because they are surely present in the beam and the lithium dimer has an absorption band system due its A–X transition with many lines around 671 nm: for most rovibrational levels of the X state, the absorption transition which is closest to the laser frequency has a very large detuning of the order of hundreds to thousands of GHz and the intensity of this resonance transition is also weaker than the resonance transition of lithium atom, because of the Franck-Condon factor. Therefore, the lithium dimers have a negligible probability of diffraction and do not contribute to the interferometer signals.

The interference signals in a Mach-Zehnder interferometer are given by:

$$I = I_0\left[1 + \mathcal{V}\cos\psi\right] \tag{12}$$

where the phase ψ of the interference fringes can be written:

$$\psi = p(2k_L)(x_1 + x_3 - 2x_2) + \phi. \tag{13}$$

The first term of ψ is particular to three-grating interferometers: the diffracted beam of order p by grating i has a phase dependent on the grating position x_i. In our case of laser diffraction, the grating position x_i is given by the mirror position M_i and $2k_L$ is the grating wavevector, where k_L is the laser wavevector. This phase term is very interesting because it is non dispersive and it is commonly used to observe interference fringes. In our case, we scan the position x_3 of mirror M_3 by a piezoelectric translation stage. The second term ϕ represents any phase difference between the two beams and in particular, it will represent the phase shift due to the application of an electric field on one of the two paths.

4.2 Introduction of the capacitor

In the present work, we have only used the diffraction order $p = 1$ so that the center of the two beams are separated by about 90 μm at the location of the capacitor, which is located just before the second laser standing wave. The capacitor is attached to the top of the vacuum chamber and not to the rail supporting the laser standing wave mirrors M_i: in this way, we do not increase the vibrations of the mirror positions x_i. The capacitor is held by a translation stage along the x-direction, which can be adjusted manually thanks to a vacuum feed through and a double stage kinematic mount built in our laboratory. The first stage, operated with screws, can be used only when the experiment is at atmospheric pressure while the second stage, actuated by low-voltage piezo-translators, can be adjusted under vacuum. When the septum is inserted between the two atomic paths, the atom propagation is almost not affected by its presence and, as shown in Figure 4, we have observed a fringe visibility equal $\mathcal{V} = 84 \pm 1$ % and a negligible reduction of the atomic flux.

To optimize the phase sensitivity (see a discussion in Ref. [6]), we have opened the collimation slit S_1 and the

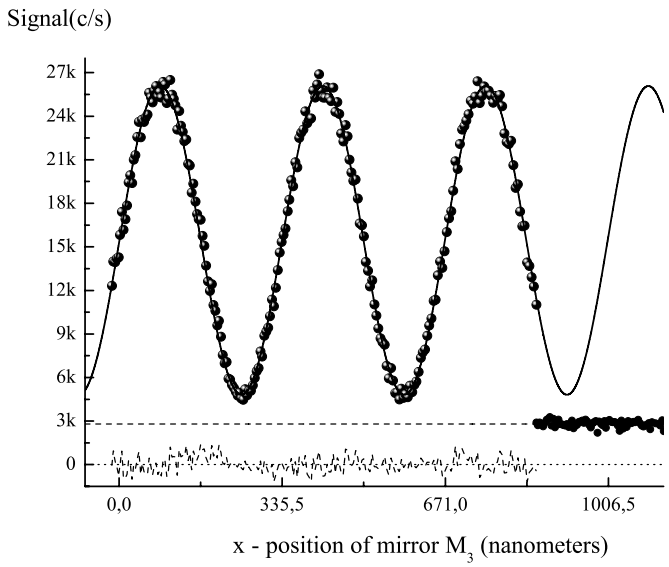

Fig. 4. Interference signal observed by displacing the mirror M_3: the signal is expressed in counts per second, but the counting time is equal to 0.1 second only and the background signal has been recorded at the end of the experiment. The full curve is the best fit and the fit residuals are plotted, at the bottom of the figure.

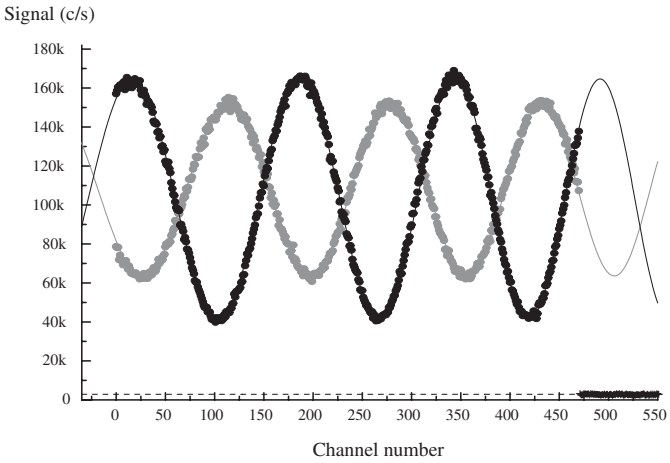

Fig. 5. Experimental signals corresponding to $V_0 = 0$ (black dots) and to $V_0 \approx 260$ volts (grey dots). Their sinusoidal fits using equation (14) are represented by the full curves. The phase shift due to the polarizability effect is close to 3π and the fringe visibility is reduced because of the dispersion of the phase shift associated to the velocity spread of the lithium atoms.

detection slit S_D (see Ref. [6]) with widths $e_1 = 18$ μm and $e_D = 50$ μm, thus increasing the mean flux up to 10^5 counts/s and slightly reducing the fringe visibility down to $\mathcal{V}_0 = 62\%$ (see Fig. 5).

4.3 The data acquisition procedure

We have made a series of recordings, labeled by an index i from 1 to 44, with $V_0 = 0$ when i is odd, and with

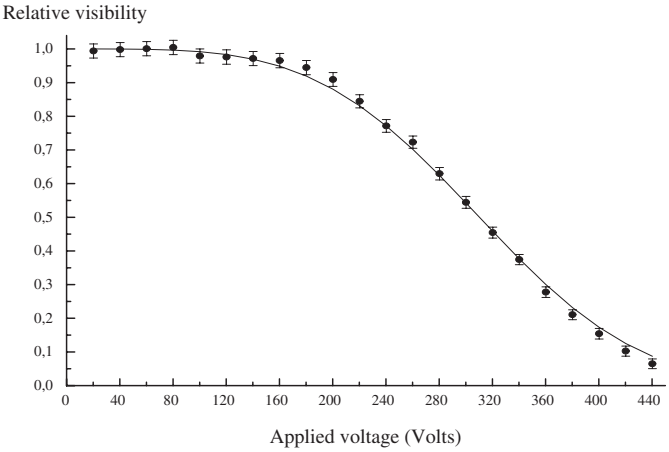

Fig. 6. Relative fringe visibility $\mathcal{V}/\mathcal{V}_0$ with $\mathcal{V}_0 = 62\%$ as a function of the applied voltage V_0. The points are our measurements and the full curve is our best fit using equations (15, 16).

$V_0 \neq 0$, when i is even with $V_0 \approx 10 \times i$ volts. For each recording, we apply the same linear ramp on the piezo-drive of mirror M_3 in order to observe interference fringes and 471 data points are recorded with a counting time per channel equal to 0.36 s. Figure 5 presents a pair of consecutive recordings.

The high voltage power supply has stability close to 10^{-4} and the applied voltage is measured by a HP model $34401A$ voltmeter with a relative accuracy better than 10^{-5}.

4.4 Extracting phases from the data

For each recording, the data points $I_i(n)$ have been fitted by a function:

$$I_i(n) = I_{0i}\left[1 + \mathcal{V}_i \cos\psi_i(n)\right]$$
$$\text{with} \quad \psi_i(n) = a_i + b_i n + c_i n^2 \tag{14}$$

where n labels the channel number, a_i represents the initial phase of the pattern, b_i an ideal linear ramp and c_i the non-linearity of the piezo-drive. For the $V_0 = 0$ recordings, a_i, b_i and c_i have been adjusted as well as the mean intensity I_{0i} and the visibility $\mathcal{V}_i$. For the $V \neq 0$ recording, we have fitted only a_i, I_{0i} and $\mathcal{V}_i$, while fixing b_i and c_i to their value b_{i-1} and c_{i-1} from the previous $V = 0$ recording. We think that our best phase measurements are given by the mean phase $\bar{\psi}_i$ obtained by averaging $\psi_i(n)$ over the 471 channels. The 1σ error bar of these mean phases are of the order of 2–3 mrad, increasing with the applied voltage up to 23 mrad because the visibility is considerably lower when the applied voltage V_0 is large (see Fig. 6). This rapid decrease of the visibility is due to the velocity dependence of the phase and to the velocity distribution of the lithium atoms.

The mean phase values $\bar{\psi}_i$ values of the $V_0 = 0$ recordings are plotted in Figure 7: they present a drift equal to 7.5 ± 0.2 mrad/minute and some scatter around this regular drift. The most natural explanation for this drift is

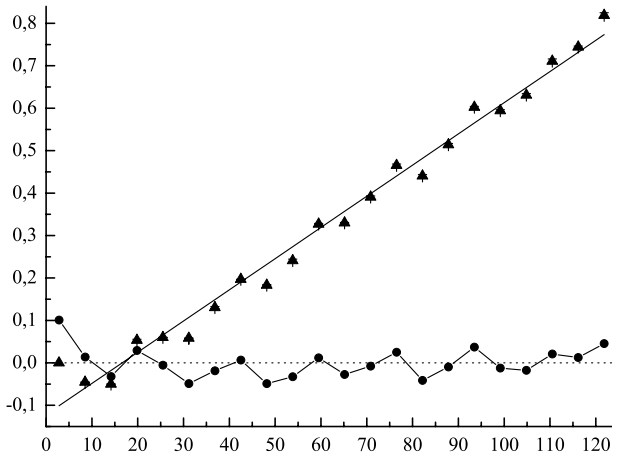

Fig. 7. The mean phase value $\bar{\psi}_i$, in radian, of the $V_0 = 0$ recordings is plotted as a function of the recording starting time t in minutes (with an arbitrary origin). The straight line is the best linear fit, corresponding to a phase drift of 7.5 ± 0.2 mrad/minute. The fit residuals are also plotted and from $t = 15$ till $t = 100$ minutes, the residuals exhibit an oscillating pattern with a period close to 17 minutes.

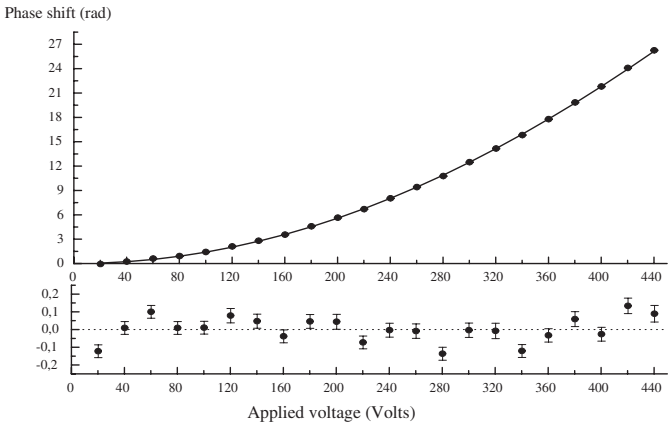

Fig. 8. The measured phase shift $\langle\phi(V_0)\rangle$ in radian is plotted as a function of the applied voltage V_0: the best fit using equations (4, 5) is represented by the full curve and the residuals are plotted in the lower graph with an expanded scale.

a change of the phase ψ resulting from a variation of the mirror positions x_i: ψ changes by 1 radian for a variation of $(x_1 + x_3 - 2x_2)$ equal to 53 nm. We have verified that the observed drift has the right order of magnitude to be due to the differential thermal expansion of the structure supporting the three mirrors: its temperature was steadily drifting at 1.17×10^{-3} K/minute during the experiment and the support of mirror M_3 differs from the other supports, as it includes a piezo translation stage, which is replaced by aluminium alloy for the mirrors M_1 and M_2. Presently, we have no explanation of the phase scatter, which presents a quasi-periodic structure as a function of time: its rms value is equal to 33 milliradians and, unfortunately, this scatter gives the dominant contribution to our phase uncertainty.

The phase shift $\langle\phi(V_0)\rangle$ due to the polarizability effect (the average $\langle\ \rangle$ recalls that our experiment makes an average over the velocity distribution, as discussed below) is taken equal to $\langle\phi(V_0)\rangle = \bar{\psi}_i - \left(\bar{\psi}_{i-1} + \bar{\psi}_{i+1}\right)/2$ where the recording i corresponds to the applied voltage V_0: the average of the mean phase of the two $V_0 = 0$ recordings done just before and after is our best estimator of the mean phase of the interference signal in zero field. In Figure 8, we have plotted the phase shift $\phi(V_0)$ as a function of the applied voltage V_0. We have chosen for the error bar on $\phi(V_0)$ the quadratic sum of the 1σ error bar given by the fit of $\bar{\psi}_i$ and the 33 milliradians rms deviation of the $V_0 = 0$ phase measurements.

5 Analysis of the signals: the effect of the lithium velocity distribution

To interpret the experimental data, we must take into account the velocity distribution of the lithium atoms.

5.1 Velocity averaging of the interference signal

We assume that this velocity distribution is given by:

$$P(v) = \frac{S_\parallel}{u\sqrt{\pi}} \exp\left[-\left((v-u)S_\parallel/u\right)^2\right] \qquad (15)$$

where u is the most probable velocity and $S_\parallel$ is the parallel speed ratio. With respect to the usual form of the velocity distribution for supersonic beams, we have omitted a v^3 factor which is traditionally introduced [25] but when the parallel speed ratio $S_\parallel$ is large enough, this v^3 has little effect and the main consequence of its omission is a slight modification of the values of u and $S_\parallel$. Here, what we consider is the atoms contributing to the interferometer signal and their velocity distribution may differ slightly from the velocity of the incident beam, as Bragg diffraction is velocity selective. The experimental signal can be written:

$$\begin{aligned} I &= I_0 \int dv P(v) \left[1 + \mathcal{V}_0 \cos\left(\psi + \phi_m \frac{u}{v}\right)\right] \\ &= I_0 \left[1 + \langle\mathcal{V}\rangle \cos\left(\psi + \langle\phi\rangle\right)\right] \end{aligned} \qquad (16)$$

where ϕ_m is the value of the phase ϕ for the velocity $v = u$. If we introduce $\delta = (v-u)/u$ and expand (u/v) in powers of δ up to second order, the integral can be taken exactly, as discussed in Appendix B. However, the accuracy of this approximation is not good enough when ϕ_m is large and we have used direct numerical integration to fit our data.

5.2 Numerical fit of the data

Using equations (15) and (16), we have fitted the measured phase ϕ and visibility $\mathcal{V}$ as a function of the applied voltage V. The phase measurements received a weight inversely proportional to the square of their estimated uncertainty and we have adjusted two parameters, the value of ϕ_m/V^2 and the parallel speed ratio $S_\parallel$. The results of the fits are

presented in Figures 8 and 6. The agreement is excellent, in particular for the phase data, and we deduce a very accurate value of ϕ_m/V_0^2:

$$\phi_m/V_0^2 = (1.3870 \pm 0.0010) \times 10^{-4} \text{ rad/V}^2 \qquad (17)$$

where the error bar is equal to 1σ. The relative uncertainty on ϕ_m/V_0^2 is very small, 0.072%, which proves the quality of our phase measurements. We also get an accurate determination of the parallel speed ratio:

$$S_{\parallel} = 8.00 \pm 0.06. \qquad (18)$$

This value of the parallel speed ratio is larger than the predicted value for our lithium beam, $S_{\parallel,Li} = 6.2$ (see above) and this difference can be explained by the velocity selective character of Bragg diffraction.

6 The electric polarizability of lithium

The lithium electric polarizability is related to the value of ϕ_m/V_0^2 by:

$$\frac{\phi_m}{V_0^2} = \frac{2\pi\epsilon_0\alpha}{u}\left[\frac{2a}{h_0^2} - \frac{2h_0}{\pi}\right]\left[1 + \frac{h_1^2}{h_0^2}\right]. \qquad (19)$$

All the geometrical parameters a, h_0 and h_1 describing the capacitor are known with a good accuracy and we deduce a still very accurate value of the ratio of the electric polarizability α divided by the mean atom velocity u:

$$\alpha/u = (2.283 \pm 0.008) \times 10^{-32} \text{ m}^2\,\text{s}. \qquad (20)$$

6.1 Measurement of the mean atom velocity

We have measured the mean atom velocity u by various techniques.

We have made measurements by Doppler effect, measured either on the laser induced fluorescence signals or on the intensity of the atomic beam which is reduced by atomic deflection due to photon recoil. In the first case, the laser was making an angle close to 49° with the atomic beam and it is difficult to measure this angle with sufficient accuracy.

In the second case, we have used a laser beam almost contra-propagating with the atoms, so that the uncertainty on the cosine of the angle is negligible. The signal appears as an intensity loss on the atomic beam and, the loss is not very large because we have used only one laser, so that the atoms are rapidly pumped in the other hyperfine state. The experimental signal is shown in Figure 9. From a fit of this data, we get a value of the mean velocity $u = 1066.4 \pm 8.0$ m/s.

We have also recorded the diffraction probability as a function of the Bragg angle, by tilting the mirror forming a standing wave. This experiment is similar to the one described in our paper [6] (see Fig. 3) but it is made with a lower power density so that only the first order

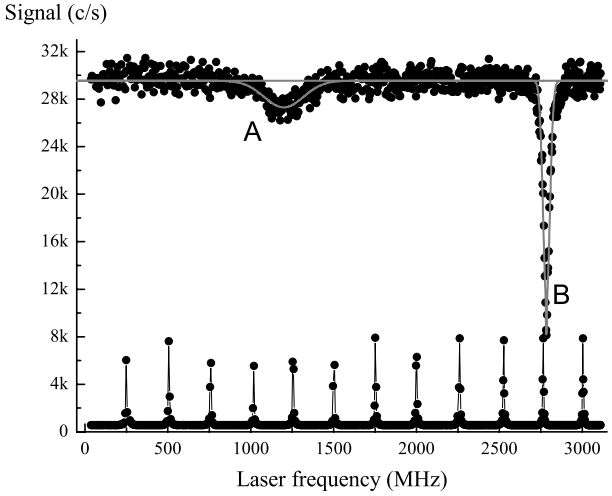

Fig. 9. Intensity losses recorded as a function of the laser frequency in MHz. The peak A corresponds to a laser beam almost contra-propagating with the atoms while the peak B corresponds to a laser beam perpendicular to the atomic beam. The lower curve is the transmission peaks of a Fabry-Perot confocal interferometer used for frequency calibration.

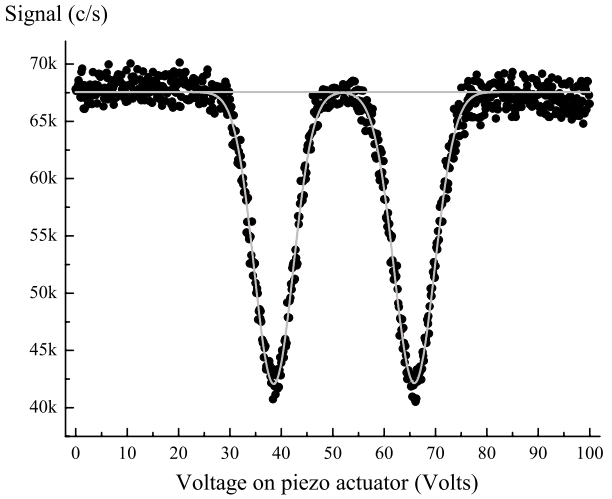

Fig. 10. Plot of the intensity of the atomic beam as a function of the voltage applied on the piezoelectric actuator inducing the rotation angle of mirror M_2. When the Bragg condition is fulfilled, the direct beam intensity is reduced by diffraction in the diffraction orders ± 1. The dots represent the measured intensity and the curves their best fit. In a separate experiment, we have calibrated the rotation angle as a function of the piezo voltage, 5.83 ± 0.03 μrad/V.

diffraction appears. The diffraction is detected by measuring the intensity of the zero-order atomic beam, as shown in Figure 10. Using an independent calibration of the mirror rotation as a function of the applied voltage on the piezo-actuator, we get a measurement of the Bragg angle $\theta_B = h/(mu\lambda_L) = 79.62 \pm 0.63$ μrad corresponding to $u = 1065.0 \pm 8.4$ m/s.

These two values are very coherent and we may combine them to give our best estimate of the most probable

velocity u:

$$u = (1065.7 \pm 5.8) \text{ m/s}. \quad (21)$$

We can compare this measurement with the theoretical prediction for supersonic expansions. For a pure argon beam, in the limit of an infinite parallel speed ratio, theory predicts $u = \sqrt{5k_BT_0/m}$ m/s where T_0 is the nozzle temperature and m the argon atomic mass. With $T_0 = 1073 \pm 11$ K, we get $u = 1056.7 \pm 5.5$ m/s. Three small corrections must be made. We must correct for the finite value of the argon parallel speed ratio $S_{\|\text{Ar}}$, estimated to be $S_{\|\text{Ar}} = 8.3$, using the semi-empirical relation of Beijerinck and Verster [23] and the associated correction reduces the most probable velocity u by a fraction equal to $0.75/S^2_{\|\text{Ar}} \approx 1.09\%$ (this correction is calculated in the limit of a vanishing perpendicular temperature [24]). We must replace the argon atomic mass by a weighted mean of the lithium and argon atomic masses and, with 0.86 mbar of lithium in 167 mbar of argon, this correction increases the velocity by 0.21%. Finally, we must take into account the velocity slip effect: the light lithium atoms go slightly faster than the argon atoms. This difference has been calculated by numerical simulation by Skovorodko [26] and this quantity is expected to scale like $S^2_{\|\text{Ar}}$, so that the correction in our case is estimated to be 2.42%. We thus predict a most probable velocity $u = 1073.0 \pm 5.6$ m/s, where the uncertainty comes solely from the uncertainty on the temperature T_0. This value is in satisfactory agreement with our measurements.

6.2 The electric polarizability of lithium

Using the measured value of the most probable velocity u, we get the lithium electric polarizability of ^{7}Li:

$$\begin{aligned}\alpha &= (24.33 \pm 0.16) \times 10^{-30} \text{ m}^3 \\ &= 164.2 \pm 1.1 \text{ atomic units}. \end{aligned} \quad (22)$$

The final uncertainty bar is equal to 0.66%, resulting from the quadratic sum of the 0.54% uncertainty on the most probable velocity u, the 0.2% uncertainty on the effective length of the capacitor, the $2 \times 0.15\%$ uncertainty due to the capacitor spacing h_0 and the 0.07% uncertainty on the interferometric measurement. Unexpectedly, the atom interferometry result has the smallest uncertainty!

Our measurement is a mean of the polarizability of the two hyperfine sublevels $F = 1$ and $F = 2$ of ^{7}Li. These two levels have not exactly the same polarizability. The difference $\Delta\alpha = \alpha(F = 2, M_F = 0) - \alpha(F = 1, M_F = 0)$ has been measured with great accuracy by Mowat [27]. We can express this result as a fraction of the mean polarizability, $\Delta\alpha = -(3.0 \pm 0.1) \times 10^{-6}\alpha$. This difference is fully negligible with our present accuracy.

Our result is in excellent agreement with those of the previous measurements of α which are considered as being reliable. The 1934 measurement of Scheffers and Stark [28], which gave $\alpha = (12 \pm 0.6) \times 10^{-30}$ m^3, is generally considered to be incorrect. The first reliable measurement is due to Bederson and co-workers [29] in 1961, who obtained $\alpha = (20.0 \pm 3.0) \times 10^{-30}$ m^3, by using the E-H gradient balance method. In 1963, Chamberlain and Zorn [30] obtained $\alpha = (22.0 \pm 2.0) \times 10^{-30}$ m^3 by measuring the deflection of an atomic beam. Finally, in 1974, a second experiment was done by Bederson and co-workers [2], using the same E-H gradient balance method improved by the calibration on the polarizability of helium atom in the $^3S_1$ metastable state, and they obtained the value $\alpha = (24.3 \pm 0.5) \times 10^{-30}$ m^3.

We may also compare our measurement with theoretical results. Many calculations of α have been published and one can find a very complete review with 35 quotations in Table 17 of the paper of King [31] published in 1997. Here is a very brief discussion of the most important results:

- the first precise calculation of α was made in 1959 by Dalgarno and Kingston [32] and gave $\alpha = 165$ a.u. This calculation was rapidly followed by several other works;
- if we forget Hartree-Fock results near 170 a.u., a large majority of the published values are in the 162–166 a.u. range;
- in 1994, Kassimi and Thakkar [33] have made a detailed study with two important results. They obtained a fully converged Hartree-Fock value, $\alpha = 169.946$ a.u. and this result, far from the experimental values, proves the importance of electron correlation. They also made a series of nth-order Möller-Plesset calculations with $n = 2, 3$ and 4, from which they extract their best estimate with an error bar, $\alpha = 164.2 \pm 0.1$ a.u.;
- in 1996, Yan et al. [34] have made an Hylleraas calculation, with the final value $\alpha = 164.111 \pm 0.002$ a.u., this value and its error bar resulting from a convergence study.

Our result is extremely close to these two very accurate calculations of α. Two minor effects have not been taken into account in these calculations, namely relativistic correction and finite nuclear mass correction, but these two effects are quite small.

The relativistic correction on the polarizability has been studied by Lim et al. [35]. They have made different calculations (Hartree-Fock, second order Möller-Plesset, coupled cluster CCSD and CCSD(T)) and in all cases, their relativistic result is lower than the non-relativistic result with a difference in the 0.05–0.07 a.u. range. We do not quote here their results: even the Hartree-Fock value is lower by 0.45 a.u. than the one of reference [33], because the chosen basis set is too small.

As far as we know, no calculation of α has been made taking into account the finite nuclear mass. An order of magnitude of the associated correction should be given by the hydrogenic approximation: $\alpha \propto [1 + (m/M)]^3$ and in this approximation, the polarizability of ^{7}Li should be larger than its $M = \infty$ value by 0.04 a.u. but one should not expect this approximation to predict even the sign of the correction. A high accuracy calculation of the finite mass effect is surely feasible, following the Hylleraas calculations of Yan and Drake, who have already evaluated

the finite mass effect on some energies [36] and oscillator strengths [37] of lithium atom.

7 Conclusion

We have made a measurement of the electric polarizability of lithium atom ^{7}Li by atom interferometry and we have obtained $\alpha = (24.33\pm0.16)\times10^{-30}$ m^3 = 164.19±1.08 a.u. with a 0.66% uncertainty. Our measurement is in excellent agreement with the most accurate experimental value obtained by Bederson and coworkers [2] in 1974 and we have reduced the uncertainty by a factor three. Our result is also in excellent agreement with the best theoretical estimates of this quantity due to Kassimi and Thakkar [33] and to Yan et al. [34]. The neglected corrections (relativistic effect, finite nuclear mass effect) should be at least ten times smaller than our present error bar.

Our measurement is the second measurement of an electric polarizability by atom interferometry, the previous experiment being done on sodium atom by Pritchard and co-workers [4] in 1995 (see also [21] and [9]). This long delay is explained by the difficulty of running an atom interferometer with spatially separated beams. Using a similar experiment, Toennies and co-workers have compared the polarizabilities of helium atom and helium dimer but this work is still unpublished [39].

We want now to insist on the improvements we have done with respect to the other measurement of an electric polarizability by atom interferometry, due to Pritchard and co-workers [4]:

- the design of our capacitor permits an analytical calculation of the E^2 integral along the atomic path. This property is important for a better understanding of the influence of small geometrical defects of the real capacitor. In the present experiment, the uncertainty on the E^2 integral is equal to 0.36% and we think that it is possible to reduce this uncertainty near 0.1% with an improved construction;
- we have obtained a very good phase sensitivity of our atom interferometer: from our recordings, we estimate this phase sensitivity near 16 mrad/$\sqrt{\text{Hz}}$. The accuracy achieved on phase measurement has been limited by the lack of reproducibility of the phase between consecutive recordings. We will stabilize the temperature of the rail supporting the three mirrors, hoping thus to improve the phase stability. Even if we have not been able to fully use our phase sensitivity, we have obtained a set of phase-shift measurements exhibiting an excellent consistency and accuracy, as shown by the quality of the fit of Figure 8 and by the accuracy, ±0.072%, of the measurement of the quantity ϕ_m/V_0^2;
- in his thesis [38], Roberts reanalyzes the measurement of the electric polarizability of sodium atom made by Ekstrom et al. [4]: he estimates that a weak contribution of sodium dimers to the interference signals can be present as material gratings diffract sodium dimers as well as sodium atoms and he estimates that, in the worst case, this molecular signal might have introduced a systematic error as large as 2% on the sodium polarizability result. Our interferometer is species selective thanks to the use of laser diffraction and this type of error does not exist in our experiment. Only lithium atoms are diffracted and even, with our choice of laser wavelength, only the ^{7}Li isotope contributes to the signal.

The main limitation on the present measurement of the electric polarizability of lithium ^{7}Li comes from the uncertainty on the most probable atom velocity u. With some exceptions, like the Aharonov-Casher phase shift [18] which is independent of the atom velocity, a phase-shift induced by a perturbation is inversely proportional to the atom velocity, at least when a static perturbation is applied on one interfering beam. This is a fundamental property of atom interferometry and clever techniques are needed to overcome this difficulty:

- Roberts et al. [9] have developed a way of correcting the velocity dependence of the phase shift by adding another phase shift with an opposite velocity dependence. They were thus able to observe fringes with a good visibility up to very large phase shift values;
- our present results prove that a very accurate measurement can be made in the presence of an important velocity dispersion without any compensation of the associated phase dispersion, but by taking into account the velocity distribution in the data analysis.

In these two cases, one must know very accurately a velocity, the most probable velocity in our case and the velocity for which the correction phase cancels in the case of reference [9]. The uncertainty on this velocity may finally be the limiting factor for high precision measurements. Obviously, other techniques can be used to solve this difficulty.

Finally, we think that our experiment illustrates well two very important properties of atom interferometry:

- the sensitivity of atom interferometry is a natural consequence of the well-known sensitivity of interferometry in general, which is further enhanced in the case of atom by the extremely small value of the de Broglie wavelength. Our phase measurement is in fact a direct measurement of the increase Δv of the atom velocity v when entering the electric field. Δv is very simply related to the observed phase shift:

$$\frac{\Delta v}{v} = \frac{\lambda_{dB}}{L_{eff}}\frac{\phi}{2\pi}. \tag{23}$$

  This variation is extremely small, with $\Delta v/v \approx 4\times10^{-9}$ for the largest electric field used in this experiment, corresponding to $\phi \approx 25$ rad. Our ultimate sensitivity corresponds to a phase $\phi \approx 3$ milliradians which means that we can detect a variation $\Delta v/v \approx 6\times10^{-13}$, whereas the velocity distribution has a FWHM width equal to 21%!
- when an atom propagates in the capacitor placed in our atom interferometer, its wavefunction samples two regions of space separated by a distance ∼90 μm with a macroscopic object, the septum, lying in between

and this situation extends over a 75 microsecond duration, without inducing any loss of coherence. This consequence of quantum mechanics remains very fascinating!

We thank CNRS SPM and Région Midi Pyrénées for financial support. We thank P.A. Skovorodko and J.L. Heully for helpful information, J.C. Lehmann, J.F. Arribart, J.F. Bobo, M. Nardone, F. Nez, F. Biraben and the staff of the AIME for their help.

Appendix A: Detailed calculation of the capacitor electric field

The first step is to calculate the Fourier transform $\tilde{V}(k)$ of $V(x=h,z)$ defined by equation (4):

$$\tilde{V}(k) = \frac{1}{\sqrt{2\pi}} \int_{-a}^{+a} V_0 \exp(-ikz)\, dz = \frac{2V_0}{\sqrt{2\pi}} \frac{\sin(ka)}{k}. \quad (24)$$

The potential $V(x,z)$ given by equation (5) can then be calculated and, from $V(x,z)$, we can deduce the electric field everywhere and in particular, on the septum surface where it is parallel to the x-axis:

$$E_x(x=0,z) = \frac{1}{\sqrt{2\pi}} \int_{-\infty}^{+\infty} \tilde{V}(k)\tilde{g}(k) \exp(ikz)\, dk \quad (25)$$

with $\tilde{g}(k) = k/\sinh(kh)$. The electric field $E_x(x=0,z)$ is given by the inverse Fourier transform of the product of two functions $\tilde{V}(k)$ and $\tilde{g}(k)$. Therefore, the field $E_x(x=0,z)$ is the convolution of their inverse Fourier transforms which are $V(x=h,z)$ and $g(z)$:

$$E_x(x=0,z) = \int_{-\infty}^{+\infty} V(x=h,z_1) g(z-z_1) dz_1. \quad (26)$$

Using reference [40] (Eq. (6) of paragraph 4.111, p. 511), we get an explicit form of $g(z)$:

$$g(z) = \frac{\pi^2}{2h^2 \cosh^2\left(\frac{\pi z}{2h}\right)}. \quad (27)$$

This result proves that the field decreases asymptotically like $\exp(-\pi|z|/h)$, when $|z| - a \gg h$. We can also get a closed form expression of the electric field $E_x(x=0,z)$ but we may get the integral of E^2 without this result, simply by using the Parseval-Plancherel theorem and reference [40] (Eq. (4) of paragraph 3.986, p. 506):

$$\int_{-\infty}^{+\infty} E_x(x=0,z)^2 dz = \frac{2aV_0^2}{h^2} \left[\coth\left(\frac{\pi a}{h}\right) - \frac{h}{\pi a}\right]. \quad (28)$$

The atoms sample the electric field at a small distance of the septum surface and we need the integral of E^2 along their mean trajectory. This mean trajectory is not parallel to the septum, but it is easier to calculate this integral along a constant x line. From Maxwell's equations, one gets the first correction terms to the field when x does not vanish:

$$E_x(x,z) \approx E_x(x=0,z) - \frac{x^2}{2}\frac{\partial^2 E_x}{\partial z^2}$$
$$E_z(x,z) \approx x\frac{\partial E_x}{\partial z} \quad (29)$$

where the derivatives are calculated for $x=0$. After an integration by parts, one gets:

$$\int_{-\infty}^{+\infty} \left[E_x^2(x,z) + E_y^2(x,z)\right] dz = \int_{-\infty}^{+\infty} \left[E_x^2(x=0,z) + 2x^2 \left[\frac{\partial E_x}{\partial z}\right]^2\right] dz \quad (30)$$

where we have kept only the first non vanishing correction term in x^2. The calculation of the integral is also done with the Parseval-Plancherel theorem and, after some algebra, we get:

$$2x^2 \int_{-\infty}^{+\infty} \left[\frac{\partial E_x}{\partial z}\right]^2 dz = x^2 \frac{V_0^2}{h^3} \left[\frac{2}{3} - \frac{\frac{\pi a}{h}\coth\left(\frac{\pi a}{h}\right) - 1}{\sinh^2\left(\frac{\pi a}{h}\right)}\right] \approx x^2 \frac{2V_0^2}{3h^3} \quad (31)$$

where the approximate result is obtained by neglecting the exponentially small terms of the order of $\exp[-2\pi h/(a)]$.

Appendix B: Velocity average of the interference signals

We want to calculate:

$$I = I_0 \int dv P(v) \left[1 + \mathcal{V}_0 \cos\left(\psi + \phi_m \frac{u}{v}\right)\right] \quad (32)$$

with the velocity distribution given by:

$$P(v) = \frac{S_\parallel}{u\sqrt{\pi}} \exp\left[-\left((v-u)S_\parallel/u\right)^2\right]. \quad (33)$$

Noting $\delta = (v-u)/u$ and expanding (u/v) in powers of δ up to second order, the integral becomes:

$$I/I_0 = \frac{S_\parallel}{u\sqrt{\pi}} \int d\delta \exp\left[-\delta^2 S_\parallel^2\right] \times \left[1 + \mathcal{V}_0 \cos\left[\psi + \phi_m\left(1 - \delta + \delta^2\right)\right]\right] \quad (34)$$

which can be taken exactly:

$$I/I_0 = [1 + \langle\mathcal{V}\rangle \cos(\psi + \langle\phi\rangle)] \quad (35)$$

$$\langle\mathcal{V}\rangle = \mathcal{V}_0 \frac{S_\parallel}{\left[S_\parallel^4 + \phi_m^2\right]^{1/4}} \exp\left[-\frac{\phi_m^2 S_\parallel^2}{4\left(S_\parallel^4 + \phi_m^2\right)}\right] \quad (36)$$

$$\langle\phi\rangle = \phi_m + \frac{1}{2}\arctan\left[\frac{\phi_m}{S_\parallel^2}\right] - \frac{\phi_m^3}{4\left(S_\parallel^4 + \phi_m^2\right)}. \quad (37)$$

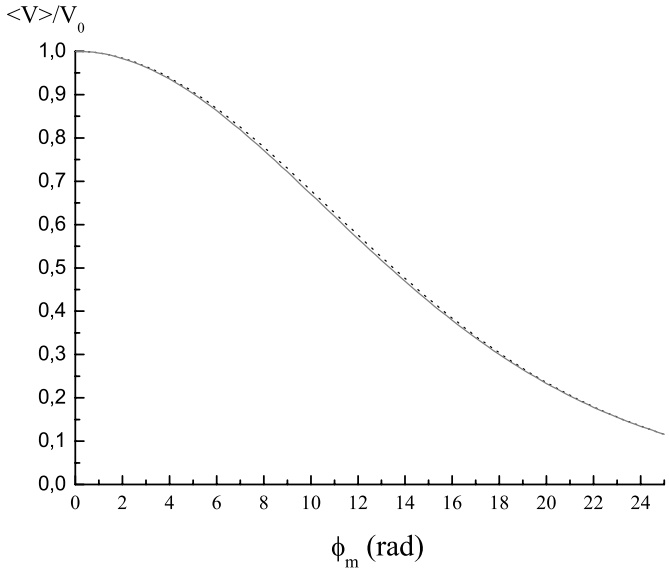

Fig. 11. Calculation of the average visibility $\langle \mathcal{V} \rangle$ in the case $S_{\parallel} = 8$ as a function of ϕ_m. The approximate result (Eq. (36)) is plotted with a dashed line while the result of the numerical integration is plotted by the full line.

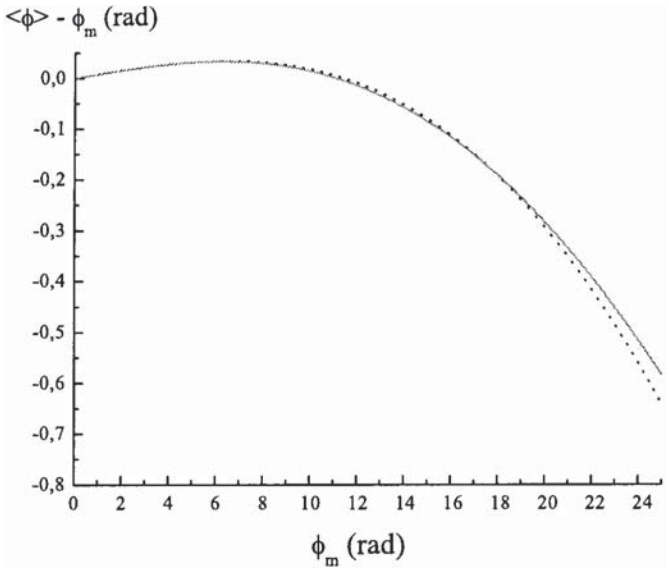

Fig. 12. Calculation of the average phase $\langle \phi \rangle$ in the case $S_{\parallel} = 8$. The quantity $\langle \phi \rangle - \phi_m$ is plotted as a function of ϕ_m: dashed line for the approximate result (Eq. (37)) and full line for the result of the numerical integration.

We have tested this approximation by comparing this approximate formula with the result of a computer program, for a parallel speed ratio $S_{\parallel} = 8$, corresponding to our experimental case. As shown in Figure 11, the agreement is very satisfactory, at least with our present accuracy on visibility values, with differences of the order of 1%.

We have also studied the difference $(\langle \phi \rangle - \phi_m)$ as a function of ϕ_m and the results are presented in Figure 12. This difference can reach large values, for instance -0.64 rad when $\phi_m \approx 25$ rad. One may remark that, as obvious on equation (37), the difference $(\langle \phi \rangle - \phi_m)$ is linear in ϕ_m and positive, when ϕ_m is small, and becomes negative and roughly cubic in ϕ_m for larger ϕ_m values. If the parallel speed ratio $S_{\parallel}$ is large, $S_{\parallel} \gg 1$, as long as the linear term is dominant, the velocity averaged phase is given by:

$$\langle \phi \rangle = \phi_m \left[1 + \frac{1}{2S_{\parallel}^2} \right] \tag{38}$$

and not by ϕ_m. With $S_{\parallel} = 8$, the approximate and numerical results are almost equal as long as $\phi_m < 18$, but their difference increases rapidly for larger ϕ_m values, being close to 0.05 radian when $\phi_m = 25$: even if this difference is a very small fraction of ϕ_m, this difference is not fully negligible and we have decided not to use the approximate analytical results (36) and (37) to fit the data.

References

1. K.D. Bonin, V.V. Kresin, *Electric-Dipole Polarizabilities of Atoms, Molecules and Clusters* (World Scientific, 1997)
2. R.W. Molof, H.L. Schwartz, T.M. Miller, B. Bederson, Phys. Rev. A **10**, 1131 (1974)
3. J.M. Amini, H. Gould, Phys. Rev. Lett. **91**, 153001 (2003)
4. C.R. Ekstrom, J. Schmiedmayer, M.S. Chapman, T.D. Hammond, D.E. Pritchard, Phys. Rev. A **51**, 3883 (1995)
5. R. Delhuille, C. Champenois, M. Büchner, L. Jozefowski, C. Rizzo, G. Trénec, J. Vigué, Appl. Phys. B **74**, 489 (2002)
6. A. Miffre, M. Jacquey, M. Büchner, G. Trénec, J. Vigué, Eur. Phys. J. D **33**, 99 (2005)
7. A. Miffre, M. Jacquey, M. Büchner, G. Trénec, J. Vigué, J. Chem. Phys. **122**, 094308 (2005)
8. A. Miffre, M. Jacquey, M. Büchner, G. Trénec, J. Vigué, Phys. Rev. A (accepted); preprint available on `https://hal.ccsd.cnrs.fr/ccsd-00005359`
9. T.D. Roberts, A.D. Cronin, M.V. Tiberg, D.E. Pritchard, Phys. Rev. Lett. **92**, 060405 (2004)
10. F. Shimizu, K. Shimizu, H. Takuma, Jpn J. Appl. Phys. **31**, L436 (1992)
11. S. Nowak, N. Stuhler, T. Pfau, J. Mlynek, Phys. Rev. Lett. **81**, 5792 (1998)
12. S. Nowak, N. Stuhler, T. Pfau, J. Mlynek, Appl. Phys. B **69**, 269 (1999)
13. V. Rieger, K. Sengstock, U. Sterr, J.H. Müller, W. Ertmer, Opt. Comm. **99**, 172 (1993)
14. A. Morinaga, N. Nakamura, T. Kurosu, N. Ito, Phys. Rev. A **54**, R21 (1996)
15. K. Sangster, E.A. Hinds, S.M. Barnett, E. Riis, Phys. Rev. Lett. **71**, 3641 (1993)
16. K. Sangster, E.A. Hinds, S.M. Barnett, E. Riis, A.G. Sinclair, Phys. Rev. A **51**, 1776 (1995)
17. K. Zeiske, G. Zinner, F. Riehle, J. Helmcke, Appl. Phys. B **60**, 295 (1995)
18. Y. Aharonov, A. Casher, Phys. Rev. Lett. **53**, 319 (1984)
19. Laser Cheval, website: `http://www.cheval-freres.fr`
20. D.W. Keith, C.R. Ekstrom, Q.A. Turchette, D.E. Pritchard, Phys. Rev. Lett. **66**, 2693 (1991)
21. J. Schmiedmayer, M.S. Chapman, C.R. Ekstrom, T.D. Hammond, D.A. Kokorowski, A. Lenef, R.A. Rubinstein, E.T. Smith, D.E. Pritchard, in *Atom interferometry*, edited by P.R. Berman (Academic Press, 1997), p. 1

22. D.M. Giltner, R.W. McGowan, Siu Au Lee, Phys. Rev. Lett. **75**, 2638 (1995)
23. H.C.W. Beijerinck, N.F. Verster, Physica **111C**, 327 (1981)
24. J.P. Toennies, K. Winkelmann, J. Chem. Phys. **66**, 3965 (1977)
25. H. Haberland, U. Buck, M. Tolle, Rev. Sci. Instrum. **56**, 1712 (1985)
26. P.A. Skovorodko, *24th International Symposium on Rarefied Gas Dynamics*, AIP Conference Proceedings **762**, 857 (2005) and private communication
27. J.R. Mowat, Phys. Rev. A **5**, 1059 (1972)
28. H. Scheffers, J. Stark, Phys. Z. **35**, 625 (1934)
29. A. Salop, E. Pollack, B. Bederson, Phys. Rev. **124**, 1431 (1961)
30. G.E. Chamberlain, J.C. Zorn, Phys. Rev. **129**, 677 (1963)
31. F.W. King, J. Mol. Structure (Theochem) **400**, 7 (1997)
32. A. Dalgarno, A.E. Kingston, Proc. Roy. Soc. **73**, 455 (1959)
33. N.E. Kassimi, A.J. Thakkar, Phys. Rev. A **50**, 2948 (1994)
34. Z.C. Yan, J.F. Babb, A. Dalgarno, G.W.F. Drake, Phys. Rev. A **54**, 2824 (1996)
35. I.S. Lim, M. Pernpointer, M. Seth, J.K. Laerdahl, P. Schwerdtfeger, P. Neogrady, M. Urban, Phys. Rev. A **60** 2822 (1999)
36. Z.C. Yan, G.W.F. Drake, Phys. Rev. A **52**, 3711 (1995)
37. Z.C. Yan, G.W.F. Drake, Phys. Rev. A **52**, R4316 (1995)
38. T.D. Roberts, Ph. D. thesis (unpublished), MIT (2002)
39. J.P. Toennies, private communication (2003)
40. I.S. Gradshteyn, I.M. Ryzhik, *Tables of integrals, series and products*, 4th edn. (Academic Press, 1980)